Medical Research Archives

ESMED
European Society of Medicine

OPEN ACCESS

Published: February 28, 2023

Citation: Vu V., Montes R., et al., 2023. The Effect of Mitral Valve Prostheses Design and Orientation on Left Ventricular Flow during Left Ventricular Assist Device Support, Medical Research Archives, [online] 11(2). https://doi.org/10.18103/mra.v11i2.3551

DOI: https://doi.org/10.18103/mra.v11i2.3551

ISSN: 2375-1924

RESEARCH ARTICLE

The Effect of Mitral Valve Prostheses Design and Orientation on Left Ventricular Flow during Left Ventricular Assist Device Support

Vu V.[1], Montes R.[1], Campos J.[1], *May-Newman K.[1]

[1]Bioengineering Program, San Diego State University, San Diego, CA 92182-1323, USA.

*kmaynewm@sdsu.edu

ABSTRACT

The mitral valve affects the shape and timing of incoming flow to the left ventricle of the heart, establishing a strong central jet that generates a vortex ring that conserves momentum during the cardiac cycle. When the vortex is disrupted, regions of stasis are introduced that increase blood residence time and the risk of thrombus formation. This risk is increased when multiple medical devices are combined, as occurs in the fraction of patients with mitral valve prostheses that experience heart failure and receive treatment with a left ventricular assist device (LVAD). LVADs are attached directly to the apex of the left ventricle, continuously pumping blood from the heart into the ascending aorta. While LVADs ameliorate the symptoms of heart failure, they are associated with thromboembolic events that result from disrupted blood flow. In this study, six different mitral prosthesis designs/orientations were studied in combination with LVAD support in a mock circulatory loop. Hemodynamics and the intraventricular velocity field were measured and the vortex characteristics determined. The bioprosthetic valve produced the standard flow pattern with a dominant clockwise vortex that circulated within the left ventricle before exiting through the LVAD. The tilting disk valve exhibited skewed inflow that produced a reverse vortex pattern when oriented towards the septum, which greatly increased stasis and residence time. The bileaflet valves split the incoming flow into two streams directed towards the apex but produced weaker vortices than the bioprosthesis. The results inform the surgical planning for LVAD patients with preexisting mitral prostheses, enabling concomitant repair procedures that would decrease the risk of thromboembolic events.

Introduction

The mitral valve (MV) affects the shape and timing of incoming flow to the left ventricle of the heart, facilitating momentum and energy transfer from low pressure diastolic filling to high pressure systolic outflow. Remodeling, repair and replacement of the MV can affect the geometry of inflow and disrupt the normal flow dynamics. There are roughly 100,000 new recipients of mitral replacements in the U.S. annually[1] and many these patients deteriorate further to heart failure, at which point they are candidates for heart transplantation. The average waiting time for heart transplants is 12 months, which poses a risk of mortality from worsening complications[2]. An alternative treatment for heart failure is a left ventricular assist device (LVAD), an implanted mechanical pump that increases systemic blood flow. LVADs provide short to intermediate term support for patients awaiting transplantation as well as long term support for advanced heart failure patients[3,4]. While previous studies have shown that concomitant MV repair or replacement at the time of LVAD implant does not affect short- and long-term mortality rates[5], an understanding of clinical complications and how they are linked to device positioning is lacking.

Bioprosthetic (BP), bi-leaflet (BL), and tilting-disk (TD) are different designs of MV prostheses, and each interacts distinctly with the incoming flow during diastole[6]. Previous studies have shown that the shape and orientation of MV prosthesis strongly affect the intraventricular vortex structures and transport[7,8]. For example, the BP and BL valves produce a similar vortex pattern to the normal heart, but the BL valve generates higher shear in the hinge regions which increases shear-induced platelet activation [6,9–12]. The TD valve in the septal orientation produced a reverse flow and vortex pattern, impairing LV washout and retaining shear activated fluid[7,8].

On the clinical side, each prosthesis type is linked with particular complications, e.g., higher thromboembolic risk for TD, increased bleeding rate for BL, and a higher rate of deterioration and stenosis for BP[13,14]. An important link between clinical complications and prosthesis design is the fluid dynamics as described by Virchow's triad[15]. Shear activated platelets which are subsequently exposed to regions of flow stasis are prone to aggregate, resulting in a thrombus that can embolize and cause a stroke. This phenomenon is characteristic of blood-contacting devices and carries greater risk when devices are combined, e.g. MV replacements and LVADs. During LVAD support, the interaction between the MV prosthesis and LVAD affects intraventricular flow, and likely increases the associated TE risks. Several studies have evaluated outcomes for patients with MV prostheses during LVAD support. MV thrombus has been observed in LVAD patients with pre-existing mitral BP [16,17], but not with MHV [18–21]. To further inform the link between MV prosthesis design and clinical complications during LVAD support, the LV flow dynamics were studied in a mock circulatory loop.

Methods

Experiments were performed with the SDSU cardiac simulator, a mock loop of the LVAD-assisted circulation[22,23]. Transparent models of a dilated left ventricle were fabricated from platinum-cured silicone rubber based on an idealized geometry of the human heart. A porcine valve prosthesis (26-mm Medtronic Mosaic) was placed in the aortic position. Each of the six MV models/orientations tested are shown in Figure 1B and included: a 25-mm Medtronic 305 Cinch bioprosthesis (BP), a Medtronic Hall tilting-disk mechanical heart valve (MHV) positioned with the large orifice directing flow toward the free wall (TD-F), or toward the septal (TD-S) and a Carbomedics MHV positioned at a 45° angle (BL-45), the anatomical (BL-A), and anti-anatomical (BL-AA) orientations. A HeartMate II continuous flow LVAD (HMII) was attached by inserting the inflow cannula through an apical sleeve of the silicone LV until it was flush with the LV apical border and secured with zip ties. Tygon tubing (16 mm diameter) replaced the LVAD outflow graft and was connected to the ascending aorta at a 90° angle approximately 15 mm distal to the aortic root. The assembly was immersed in a water-filled tank and attached to a Windkessel model of the systemic circulation. Pressure transducers (Abbott Transpac IV, Abbott Labs; Chicago IL) and flow sensors (Transonic Systems 10PXL and 20PXL; Ithaca, NY) placed as shown in Figure 1. High fidelity (200Hz) signals were measured for LV pressure (LVP), aortic root pressure (AoP), LVAD flow rate (Q_{LVAD}), and distal aortic flow rate (Q_{sys}) using a commercial data acquisition system (LabChart, AD Instruments). The circulating fluid was a viscosity-matched blood analog consisting of 40% glycerol and water (viscosity of 3.72 cP at 20 C) and was seeded through the left atrial chamber with 20-μm neutrally buoyant fluorescent particles during imaging.

Figure 1 A

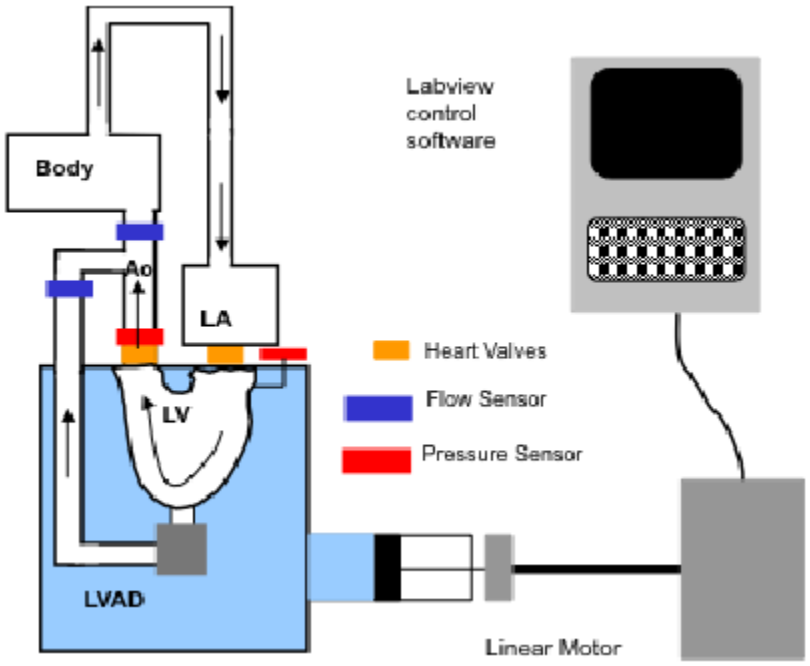

Figure 1 B

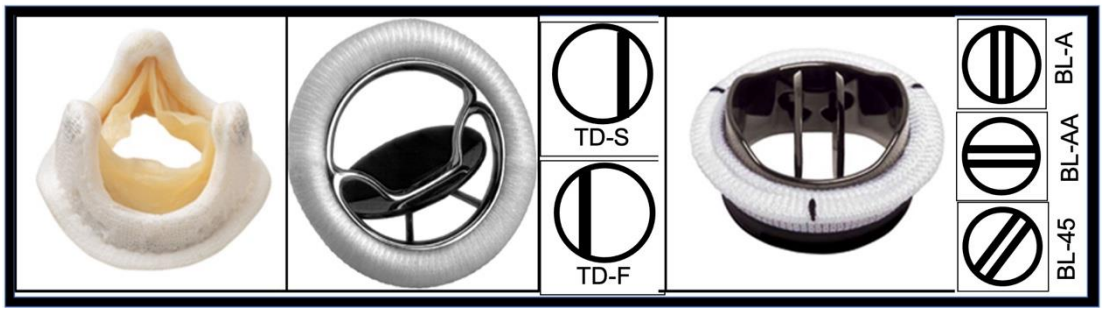

Figure 1: (A) The SDSU cardiac simulator is a mock circulatory loop that reproduces the fluid dynamics of the dilated cardiomyopathy (DCM) heart. The left ventricle is a silicone rubber model positioned with a left ventricular assist device (LVAD) attached inside of a transparent fluid-filled chamber. (B) Three mitral valve prostheses were tested in different orientations under matched hemodynamic conditions (from left to right): porcine bio-prosthesis (BP); tilting disk mechanical heart valve (MHV) in the septal (TD-S) (top), and free wall (TD-F) (bottom) orientations; bileaflet MHV in anatomical (BL-A) (top), anti-anatomical (BL-AA) (middle), and 45° angle (BL-45) (bottom) orientations.

A laser light sheet 1-2 mm in thickness focused on the long-axis plane of the LV illuminated the particles within the LV model while a LaVision Digital Particle Image Velocimetry system (LaVision, Inc) captured 12-bit digital images with a time interval of 700-2000μs. Interrogation windows of 32x32 applied to a field of 1376x1040 pixels obtain a spatial resolution of 14 pixels/mm. Triggered image pairs were acquired at 40 Hz for each condition and phase averaged. A mask corresponding to the LV boundary was

generated at each time frame and applied to remove the image background. The image field was calibrated using a grid with 2-mm spacing covering the field of view and the two-dimensional velocity field v(x,y,t) obtained for a single cardiac cycle for each condition.

A Pre-LVAD patient with an ejection fraction of 20% was established with the LVAD off and the LVAD outflow conduit clamped. The Pre-LVAD settings for the cardiac simulator achieved a mean aortic pressure of 57 mmHg and a cardiac output of 2.54 L/m (corresponding to a 20% ejection fraction) at a heart rate of 72 bpm, representing a NYHA Class IV heart failure patient [24,25]. Two different HMII LVAD speeds were tested: 8000 (low) and 11,000 (high) rotations per minute (rpm).

Data Analysis

For the hemodynamic parameters, ten cardiac cycles recorded during the imaging period were downsampled to 10 Hz for each flow condition and averaged. The aortic pulsatility index (PI) was calculated as the range (maximum - minimum) of Q_{sys} divided by the average for 10 cardiac cycles.

Image Analysis

A single representative cardiac cycle was calculated from the ensemble-averaged image sequence. Velocity field data v(x,y,t) were analyzed to calculate regional flow stasis, vortex dynamics and other surrogate markers of thromboembolic event risk. Small user-defined regions of interest (ROIs) of at least 50 pixels were selected at the MV, aortic valve and LVAD inflow cannula as shown in Figure 2 and the average velocity computed during the cardiac cycle. The velocity profile along the line located 20 mm from the MV annulus was computed at the peak of E- and A- wave for six types of prosthesis valves during 8k and 11k LVAD support. The velocity of inflow toward the left ventricular apex was designated as positive, while the flow toward the aortic valve (away from the apex) was designated as negative.

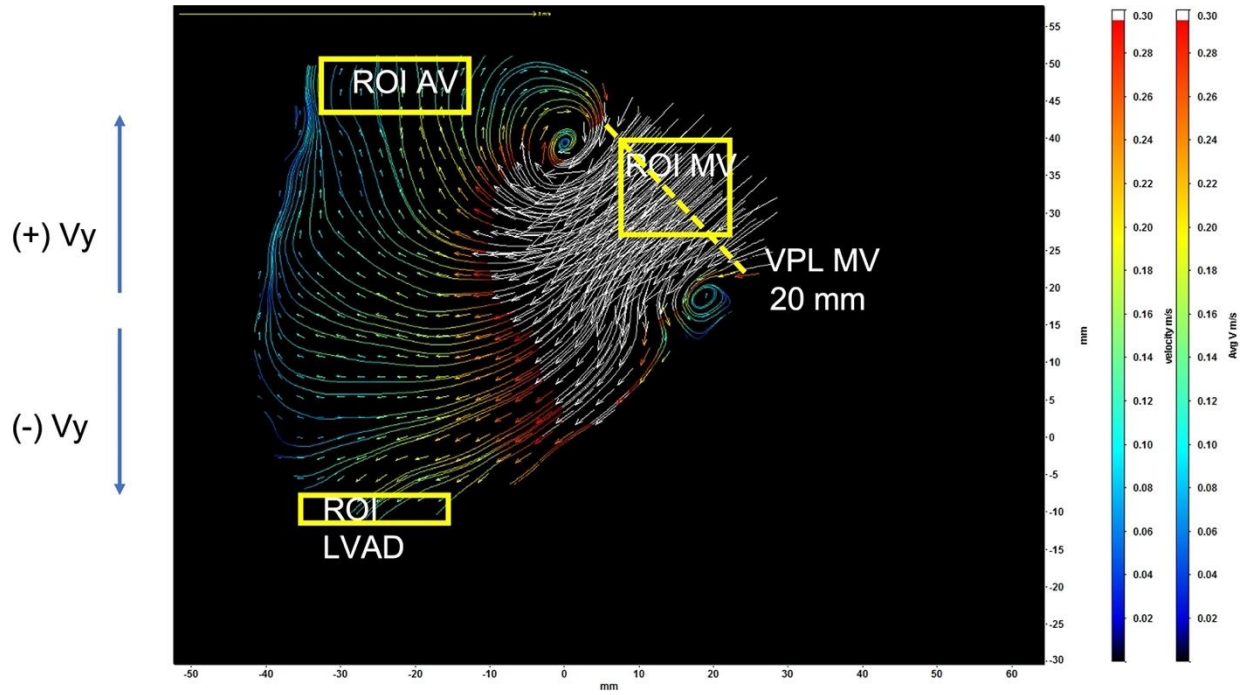

Figure 2. Image analysis of the velocity field included regions of interest (ROI) used to calculate the average y-component velocity (Vy) as a function of time during the cardiac cycle at the mitral valve (MV) inlet, aortic valve (AV) outlet and left ventricular assist device (LVAD) outlet. The positive (+) and negative (-) directions defined for Vy are shown in the diagram.

Vortices were identified in the recorded velocity fields and their dynamical properties tracked as previously described[22,26]. Vortex identification enables visualization and quantification of swirling coherent structures. In two dimensions, the three-dimensional LV vortex ring is visualized as two cores corresponding to the intersections between the mitral vortex ring and the imaging plane, one rotating in the clockwise (CW) direction and the other in the counter-clockwise (CCW) direction.

Blood Residence Time

Blood residence time (T_R) was determined using the modified advection equation, as described in detail in previous publications[6,27]. The equation was integrated in time for twenty cardiac cycles, which ensured convergence to a periodic solution.

Statistical Analysis

The hemodynamics properties (LVP, AoP, Q_{sys}, Q_{LVAD} and Aortic PI) for different valve prostheses at 8k and 11k rpm LVAD speed were tested for normality using the Shapiro-Wilk test. A Kruskal-Wallis one-way ANOVA test was used to assess the statistical significance for the 8k and 11k groups, and the Wilcoxon Rank-Sum test with Bonferroni correction used for pairwise comparisons. Significance was achieved for $p \leq 0.01$.

Results

Six combinations of MV prosthesis design and orientation were tested for a cardiac

ejection fraction of 26% and two different speeds of LVAD support (8 and 11 krpm). At the lowest LVAD speed, mean aortic pressure was maintained at 83 ± 3 mmHg. When LVAD speed was increased, the mean aortic pressure increased to 118 ± 4 for all valve conditions. The mean flow rate through the LVAD and aortic valve varied somewhat across the different valve designs and orientations as shown in Table 1. As LVAD speed changed from 8 to 11 krpm, the AoP, Q_{LVAD}, and Q_{sys} increased by 42%, 80%, and 26%, respectively while aortic PI decreased by 54%. The fraction of total cardiac output exiting the LV through the LVAD can be calculated from the ratio of Q_{LVAD} to Q_{sys} and increased from 60-70% at 8 krpm to over 90% at 11krpm.

Table 1. Bulk flow and pulsatility index (PI) averages (± SE) for 10 cycles measured for each valve and LVAD speed condition.

Condition		Q_{sys} (L/min)	Q_{LVAD} (L/min)	Aortic PI
LVAD Speed 8 krpm	BP	4.14 ± 0.14	2.65 ± 0.01	3.68
	TD-F	4.31 ± 0.01	2.54 ± 0.01	3.75
	TD-S	4.48 ± 0.01	2.83 ± 0.00	4.16
	BL-AA	4.05 ± 0.01	2.95 ± 0.01	3.25
	BL-A	4.34 ± 0.01	2.98 ± 0.01	3.38
	BL-45	4.24 ± 0.01	2.81 ± 0.01	3.66
		Q_{sys} (L/min)	Q_{LVAD} (L/min)	Aortic PI
LVAD Speed 11 krpm	BP	5.20 ± 0.01	4.89 ± 0.01	1.49
	TD-F	5.28 ± 0.01	4.75 ± 0.01	1.79
	TD-S	5.62 ± 0.01	5.14 ± 0.00	1.99
	BL-AA	5.24 ± 0.01	4.95 ± 0.01	1.52
	BL-A	5.50 ± 0.01	5.33 ± 0.01	1.46
	BL-45	5.33 ± 0.01	5.07 ± 0.01	1.71

The velocity fields in the LV mid-plane for selected instants of the cardiac cycle are shown in Figures 3-5, illustrating the flow dynamics produced by each valve case for LVAD support at 11krpm. As reported in previous studies, the LV flow patterns observed in patients with dilated cardiomyopathy reflect characteristic features. The BP valve (Figure 3) is the only prosthesis with a trileaflet design that features a central orifice and serves as the baseline for physiological comparison. BP valve inflow in early diastole (E-wave) is reduced during LVAD support, compared to the same contractility condition when no LVAD support is present. When the MV opens, a vortex ring forms that elongates toward the septum and attenuates towards the free wall. The vortex

ring asymmetry is quantified from the 2-D midplane which captures the cross section as two counter-rotating vortices. The CW vortex is larger than the CCW vortex, and exhibits greater vortex circulation and kinetic energy. During diastolic filling, the CW vortex first moves toward the LV center and then changes direction towards the aortic valve. At the same time, the CCW vortex travels along the free wall towards the apex and the LVAD inflow cannula. A smaller vortex ring forms during atrial contraction (A-wave) that reinforces the same vortex trajectories as illustrated in Figure 3.

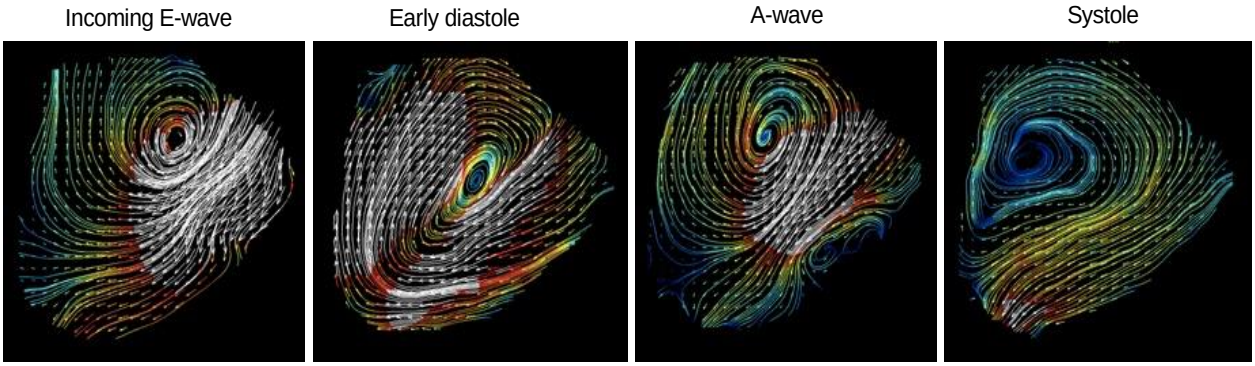

Figure 3. The bioprosthetic heart valve most closely replicates the large central orifice of the native valve, which creates the asymmetric vortex ring that dominates diastolic flow. During systole, the flow exists through the apical LVAD rather than the native aortic valve.

The tilting disc design has two orifices of unequal size that create a biphasic velocity profile and predispose asymmetry of the mitral vortex ring that forms in early diastole. As shown in Figure 4, the two orientations of the TD mechanical valve show skewed inflow velocity distributions, with large velocity gradients across the width of the prostheses. These gave rise to multiple E-wave vortices that merged during the A-wave. When the bigger orifice was directed toward the free wall (TD-F), the incoming flow becomes entrained in the larger vortical flow within the LV and contributes to maintaining the fluid momentum. The TD-F valve exhibited a strong inflow jet attached to the lateral wall and a more persistent CW vortex than the BP valves. This pattern is reflected in the velocity profiles, which were not symmetric and peaked toward the free-wall. When the larger orifice was directed toward the septum (TD-S), mitral inflow forms a strong CCW vortex that pushes the incoming flow towards the septum where it lost momentum. The dominant and persistent CCW vortex resulted in a complete reversal of the normal flow pattern and increased residence time.

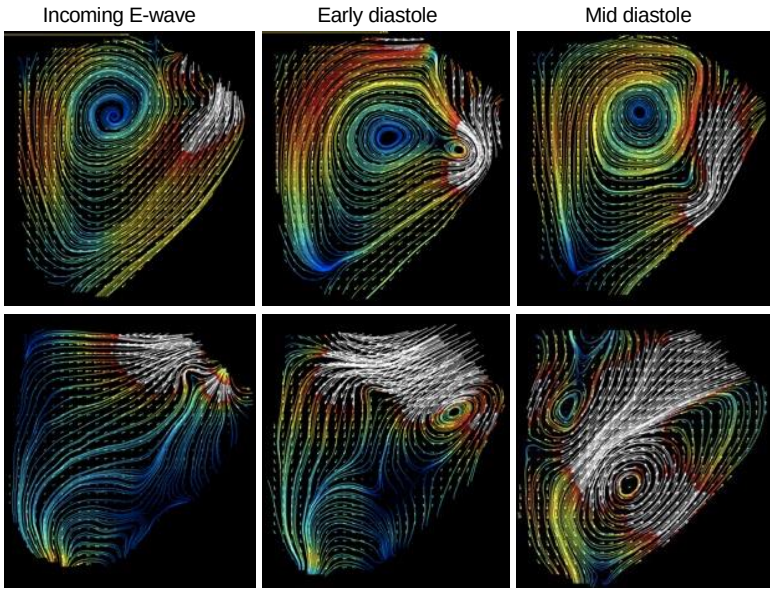

Figure 4. The tilting-disk mechanical heart valve produces asymmetric inflow when the larger orifice is oriented towards the free wall (top row) or septum (bottom row). The free wall orientation produces a large CW vortex while the septal orientation results in a reversed vortex pattern, in which the incoming flow crosses the path of the flow exiting through the aortic valve.

The bileaflet or "butterfly" valve design opens into three separated regions as shown in Figure 1B. The BL design altered the diastolic flow pattern through the MV, although the overall swirling motion of blood was less affected (Figure 5). Depending on the orientation of the valve, the midplane reflects the intersection of the three flow streams. The BL-A exhibited distinct vortex formation during early diastole and velocity inflow profiles with two distinct peaks corresponding to the two large openings. These two separate flow streams penetrate the left ventricle, allowing the CW vortex to develop normally but the CCW vortex is attenuated. During the E-wave, the CW vortex moved toward the center then changed direction toward the MV, opposite to the normal motion of the CW vortex. The CCW vortex moved towards the apex and was reinforced by the A-wave flow. Low LVAD support produced higher E-wave velocities while the A-wave profiles were roughly for both LVAD speeds. The BL-AA orientation exhibits a large central flow in the midplane that forms a vortex ring in early diastole and follows a similar trajectory to the BL-A pattern (Figure 4), but with lower energy as seen in Table 2.

Table 2. A. Intraventricular vortex properties and B. ANOVA pairwise comparisons summary for six MV prostheses flow conditions during LVAD speeds of 8 and 11 krpm.

A.

Vortex Properties 8k LVAD		BP	TD-F	TD-S	BL-AA	BL-A	BL-45
Total Kinetic energy (mJ/m)		3.26 ± 0.72	3.37 ± 0.39	2.86 ± 0.63	3.31 ± 0.65	2.02 ± 0.25	2.04 ± 0.37
Kinetic energy (mJ/m)	CW† 5**, 8*, 9*, 12**, 14**, 15**	2.54±0.56	2.93±0.31	1.01±0.35	2.43±0.40	1.57±0.17	1.32±0.19
	CCW† 5**, 8**, 9**, 12**, 14**, 15**	0.72±0.26	0.44±0.11	1.84±0.36	0.89±0.32	0.46±0.09	0.72±0.19
Circulation ($x10^{-3}$ m^2/s)	CW† 4**, 5**, 8**, 9**, 11, 12**, 14**, 15**	21.78±2.57	30.60±2.20	6.24±1.28	22.65±1.80	20.22±0.97	17.78±1.17
	CCW† 5*, 8*, 9*, 11*, 12**, 14*, 15*	-4.70±0.96	-4.17±0.72	-20.25±1.62	-7.21±0.86	-4.66±0.74	-6.54±1.12
Radius (cm)	CW† 3, 4**,5**, 8**, 9**, 10*, 11**, 12**, 14**, 15**	0.73±0.04	0.97±0.05	0.40±0.02	0.82±0.05	0.76±0.04	0.73±0.04
	CCW† 5**, 7*, 8**, 9**, 11, 12**, 14**, 15**	0.30±0.01	0.26±0.01	0.74±0.04	0.24±0.01	0.31±0.01	0.35±0.01
Aspect Ratio	CW† 12, 14*, 15*	1.62±0.08	1.51±0.06	1.85±0.10	1.65±0.08	1.58±0.06	1.50±0.06
	CCW†	1.62±0.07	1.57±0.09	1.78±0.09	1.84±0.08	1.45±0.07	1.48±0.08
Vortex symmetry CW:CCW† 5**, 7**, 8**, 9**, 10**, 11**, 12**, 14**, 15**		2.56±0.19	3.77±0.31	0.76±0.09	3.60±0.25	2.20±0.13	2.04±0.18

B.

Vortex Properties 11k LVAD		BP	TD-F	TD-S	BL-AA	BL-A	BL-45
Total Kinetic energy (mJ/m) † 3**, 7**, 10**, 13**, 14**		3.09 ± 0.70	3.06 ± 0.40	3.23 ± 0.70	0.66 ± 0.15	2.07 ± 0.25	2.02 ± 0.31
Kinetic energy (mJ/m)	CW† 2, 3**, 5*, 7**, 8**, 9**, 10**, 11*, 12**, 13**, 15**	2.47±0.55	2.56±0.30	1.08±0.42	0.49±0.11	1.58±0.19	1.40±0.17
	CCW† 5**, 9**, 10*, 11*, 12**, 14**, 15**	0.62±0.17	0.19±0.05	2.05±0.37	0.21±0.08	0.54±0.09	0.64±0.15
Circulation ($x10^{-3}$ m^2/s)	CW† 3**, 5**, 7**, 8*, 9**, 10**, 11**, 12**, 13**, 15**	21.29±2.41	27.03±2.06	6.31±1.53	9.00±1.11	19.27±0.94	18.41±0.93
	CCW† 2*, 5, 8*, 9*, 10, 11**, 12*, 14**, 15*	-4.20±0.58	1.86±0.42	-21.12±1.90	-2.83±0.52	-5.10±0.64	-6.31±1.09
Radius (cm)	CW† 3**, 4**, 5*, 7**, 8**, 9**, 12**, 14**, 15**	0.71±0.04	1.04±0.05	0.46±0.03	1.05±0.05	0.87±0.05	0.85±0.05
	CCW† 5**, 9*, 12**, 14**, 15**	0.27±0.01	0.30±0.03	0.90±0.06	0.38±0.06	0.35±0.02	0.40±0.03
Aspect Ratio	CW†	1.60±0.08	1.62±0.05	2.06±0.19	1.68±0.10	1.64±0.06	1.54±0.06
	CCW†	1.76±0.11	1.89±0.24	2.07±0.10	2.54±0.41	1.68±0.08	1.76±0.19
Vortex symmetry CW:CCW† 5**, 9**, 12**, 14**, 15**		2.86±0.19	3.58±0.37	0.74±0.11	3.47±0.39	2.55±0.24	2.46±0.25

Average ± standard error for the cardiac cycle; CW: clockwise, CCW: counter clockwise vortex core.
† Statistical significance ($p < 0.05$) for mitral valve prosthesis design.
ANOVA pairwise comparisons:
[1]BP vs. BL-45 [2]BP vs. BL-A [3]BP vs. BL-AA [4]BP vs. TD-F [5]BP vs. TD-S
[6]BL-45 vs. BL-A [7]BL-45 vs. BL-AA [8]BL-45 vs. TD-F [9]BL-45 vs. TD-S
[10]BL-A vs. BL-AA [11]BL-A vs. TD-F [12]BL-A vs. TD-S
[13]BL-AA vs. TD-F [14]BL-AA vs. TD-S
[15]TD-F vs. TD-S
Significance codes: 0 '**' 0.001 '*' 0.01 ' '

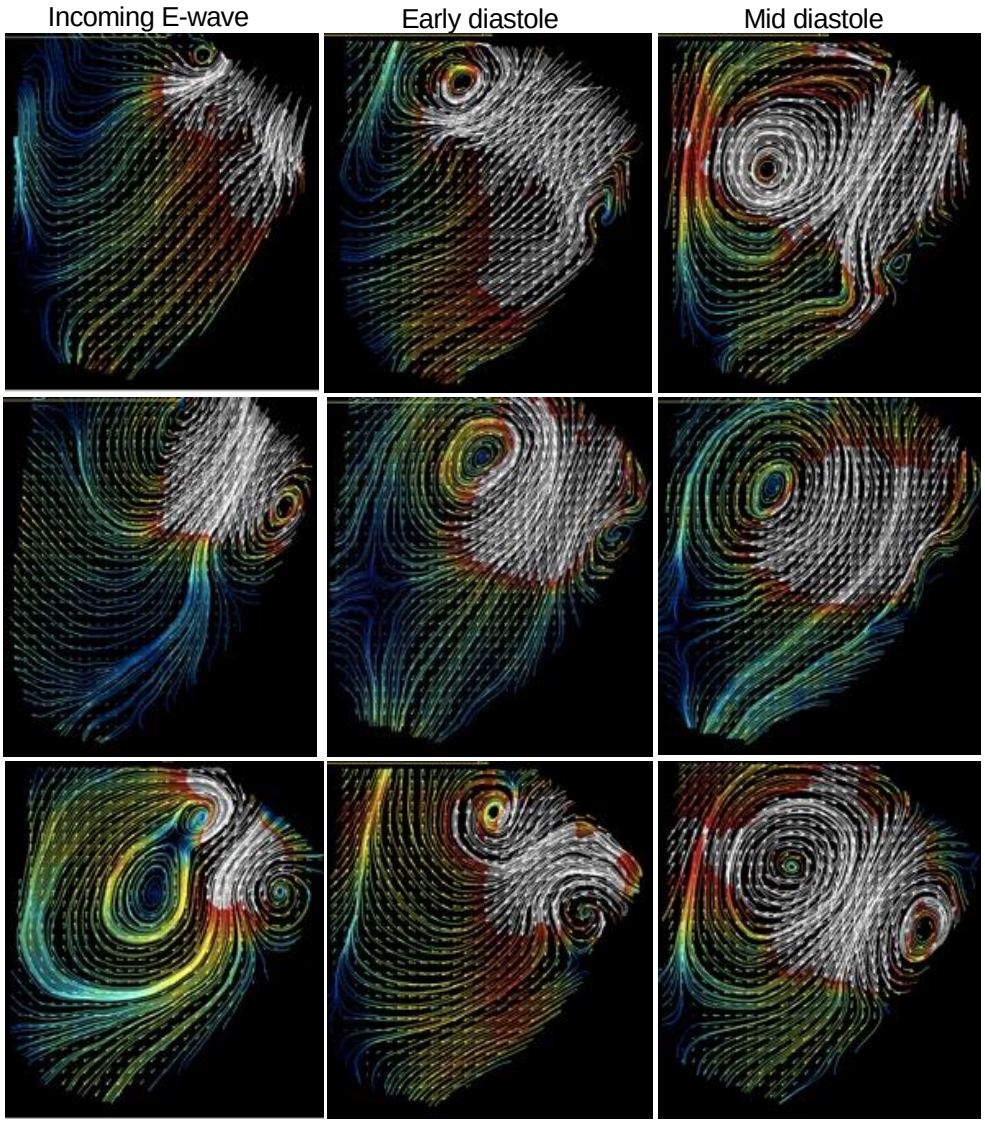

Figure 5. The bileaflet mechanical heart valve has a narrow central and two larger passages which can be oriented parallel, perpendicular, or at an angle to the midline. The anatomical orientation (top row) exhibits two flow peaks generated by the larger passages, which the other two orientations (anti-anatomical, middle row; 45° angle, bottom row) produce asymmetric vortex rings similar to the standard pattern of the bioprosthesis.

During the A-wave, the inflow velocity profile is shifted toward the free wall and the CCW vortex forms while the CW vortex is not visible. The BL-45 orientation is rotated with the larger section towards the LV center, producing an asymmetric inflow velocity profile during the E- and A-waves as displayed in Figure 6.

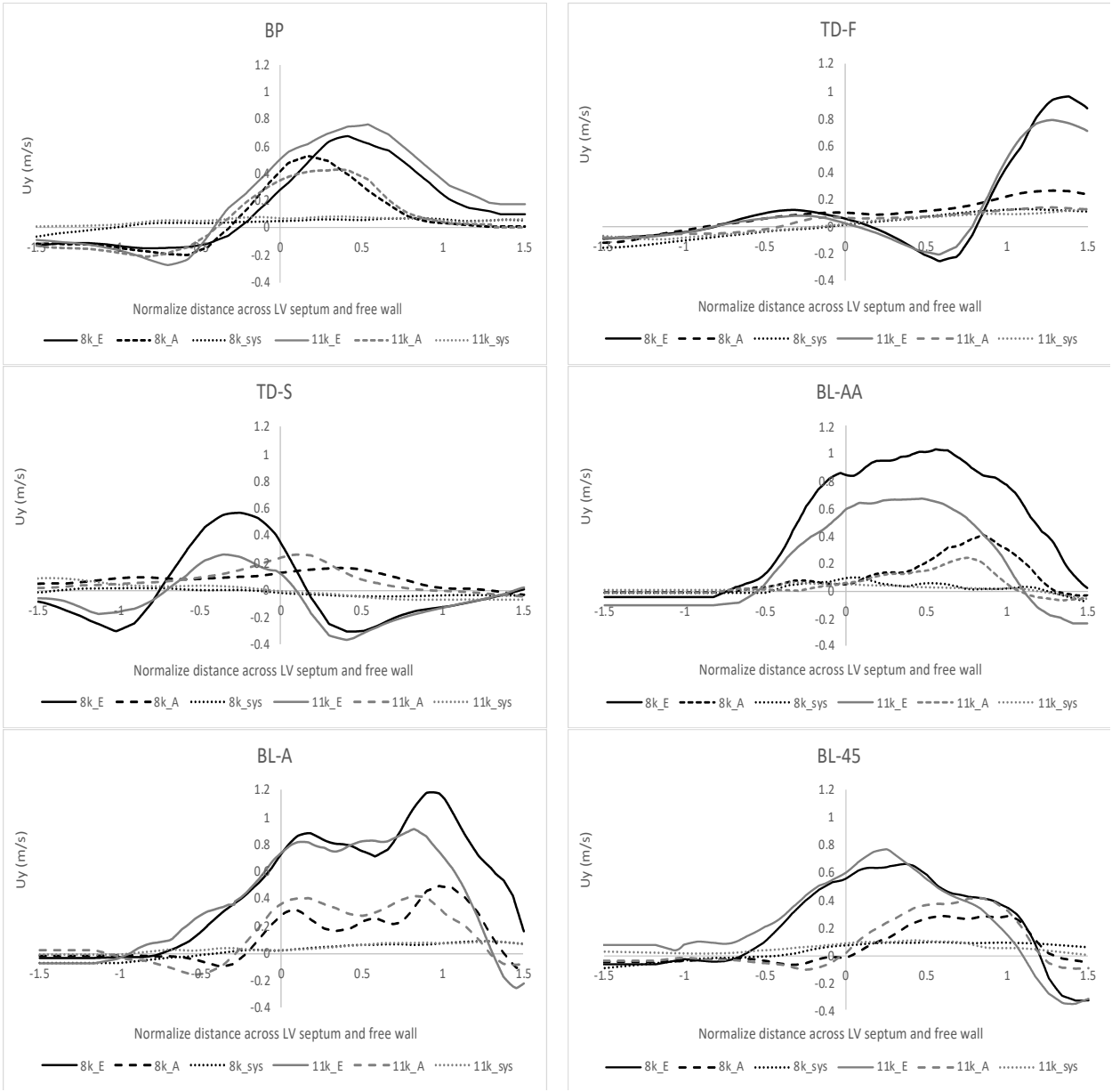

Figure 6. Vertical y-component velocity profiles along the lines 20 mm from and parallel to the MV annulus, at peak E and A wave inflow during 8 krpm and 11 krpm LVAD support for the six MV prosthesis cases.

The CW and CCW vortices form and move along the trajectories depicted in Figure 7, with similar circulation and energy characteristics as the BL-A orientation. The inflow velocity profile exhibits a parabolic shape with a reduced magnitude compared to the same condition without LVAD support[6].

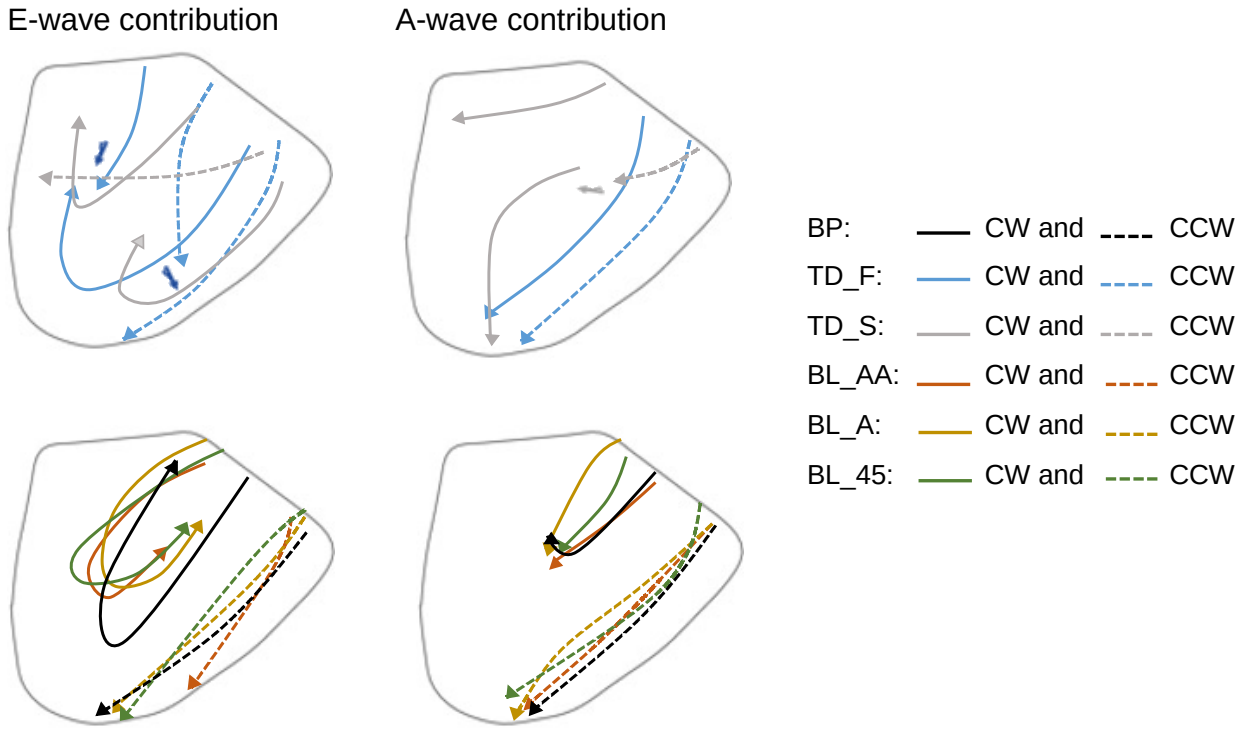

Figure 7. Vortex core trajectories as the result of the E-wave and A-wave inflow contributions are shown for six orientations of MV prostheses during 11 krpm LVAD support: clockwise (CW) and counterclockwise (CCW) (symbol indicates the merging to vortices).

Blood Residence Time

T_R maps of the LV following 20 cardiac cycles are shown in Figure 8 for the different valve designs and configurations and both LVAD speeds. The BP case exhibited the lowest T_R, with no regions with residual area (T_R > 2 s) during different LVAD support levels. At the low LVAD support level, T_R of BL-AA was slightly worse than the BP valve but had no residual area. The BL-A, BL-45, and TD-F had a relatively similar T_R. The residual area of BL-45 is lowest among those three, spreading along the LVOT. The BL-A has the largest residual area, mostly confined to the LV center, while the TD-F valve residual area was localized underneath the AV base and in the LV center. The reversed swirling pattern introduced by the TD-S valve impaired LV washout, leading to the highest T_R and region with $T_R \geq 5$ s at the MV base. During high LVAD support, BL-A had a significant reduction in T_R and residual area, followed by the TD-F case as reported in Table 3. The other BL cases, however, had higher average times and some T_R region ≥ 2 s. The TD-S T_R increased dramatically (more than 3-fold), covering approximately 90% of the LV midplane area.

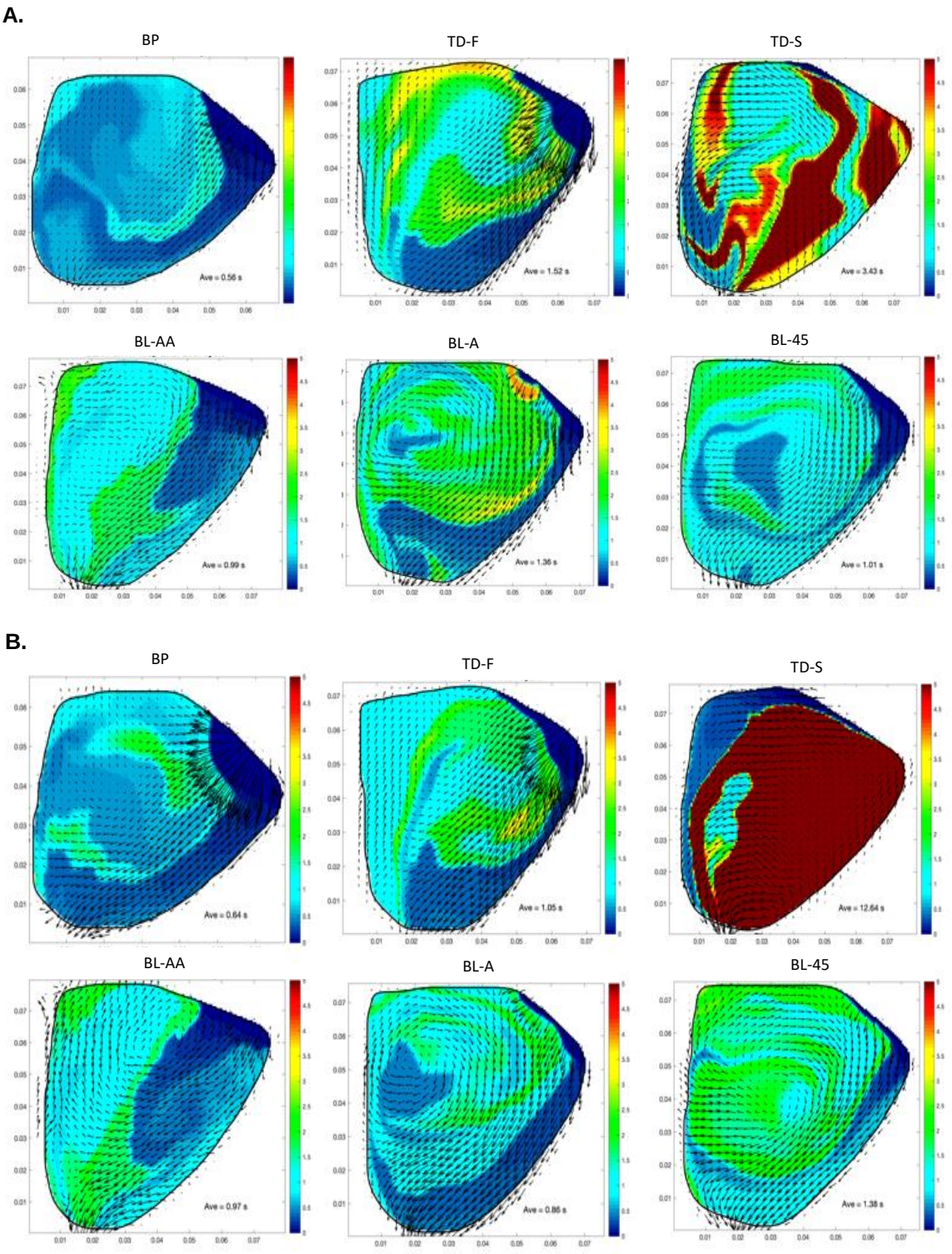

Figure 8. Residence time (RT) maps for each valve condition during 8krpm LVAD support after the 20th cardiac cycle. The average RT is shown in each frame. A. LVAD speed of 8krpm B. LVAD speed of 11 krpm.

Table 3. Residence time and transport characteristics for the six valve conditions and two LVAD speeds.

Condition		Tr_ave (s)	% of area > 2 s (%)	Average Tr of area > 2 s
LVAD Speed 8 krpm	BP	0.56	N/A	N/A
	TD-F	1.52	33.99	2.43
	TD-S	3.43	52.89	3.05
	BL-AA	0.99	N/A	N/A
	BL-A	1.36	66.84	2.32
	BL-45	1.01	16.06	2.08
LVAD Speed 11 krpm	BP	0.64	N/A	N/A
	TD-F	1.05	21.24	3.21
	TD-S	12.64	89.10	7.56
	BL-AA	0.97	N/A	N/A
	BL-A	0.86	9.00	1.92
	BL-45	1.38	47.15	2.82

Discussion

This study presents a side-by-side comparison of intraventricular flow patterns generated by different MV prosthesis designs and orientations in an *in vitro* dilated heart failure model during LVAD support. Under these conditions, the BP valve produced the most efficient left ventricular washout due to the high inflow jets and strong CW vortex circulation limiting stasis flow formation. The BP also exhibited the lowest T_R in comparison to other valve types and positions, although LVAD support slightly increased T_R and introduced some region of high T_R near the MV. In contrast, the TD-S case exhibited a reverse vortex pattern with a large CCW flow swirl causing a collision of the inflow and outflow jets, which were previously linked to lower mechanical efficiency and higher risk of thromboembolic events[8,28], and heavily impacted LV flow transport as reflected in the high T_R associated with TD-S. The TD-F case produced a flow pattern that enhanced T_R through better apical washout during LVAD support, with the large inflow jet producing the asymmetric vortex pattern associated with normal LV flow. Regions of flow stasis, shown in red, were mostly localized near the AV base and LV center during low LVAD support. However, they expanded to spread along the left ventricular outflow tract and towards the MV, potentially posing a risk of ventricular and valvular thrombosis. For the BL valves, increasing LVAD support improved flow mixing and transport, resulting in lower average T_R in the anatomical position, but increased T_R and introduced residual flow regions along the left ventricular outflow tract in the anti-anatomical and 45° positions.

Characterization of the intraventricular flow field, including vortex dynamics, and T_R provides insight into assessing the risk of thromboembolic risk. Diastolic vortical flow in the LV was first observed back in 1995 and has been extensively studied and characterized[22,29–31]. Inflow through the native

MV produces a vortex ring which grows asymmetrically due to the shape of the left ventricle. As viewed in the midplane, the cross-section of the ring shows two counter-rotating vortex cores on either side of the MV. The vortex adjacent to the free wall rotates in the CCW direction and dies along the wall as diastole progressed, but the CW vortex core grows in size as mitral inflow is redirected towards the aortic valve[32] resulting in efficient filling and limited dissipated energy[29]. The flow pattern is significantly altered in dilated cardiomyopathy (DCM) due to changes in left ventricular geometry and function that affect blood transit and vortex formation[26,33,34]. The vortex dynamics of DCM patients showed a well-rounded CW vortex near the MV, causing lower velocity propagation and favoring stasis flow at the LV apex[26]. Echocardiographic assessment reported that DCM hearts demonstrated larger CW vortex circulation and kinetic energy than healthy hearts[35]. Large residual volume has been found in DCM patients[36] and linked to thrombosis in acute myocardial infarction[26,37].

As described previously, MV design greatly impacts the resulting intraventricular flow by shaping the diastolic inflow[38]. The large central orifice of the BP design produces a single high velocity jet that generates the characteristic vortex ring. A misaligned BP or the TD with the large orifice oriented toward the septum creates a reverse vortex pattern, and the BL design splits the incoming flow in two, reducing the strength of the diastolic vortex (see Figure 9). These patterns are also influenced by mitral repair procedures such as annuloplasty and Mitraclip placement. Surgical MV repair has emerged as a viable alternative to replacement in selected cases. Mitral regurgitation can be addressed with ring annuloplasty, in which the mitral annulus is sutured to a stiff ring to decrease the orifice diameter. The procedure produces a smaller orifice that results in a higher velocity inflow, similar to the BP valve replacement[38]. MV prolapse may be treated with a MitraClip (Abbott Laboratories Inc), and effectively splitting the incoming flow into two jets that dissipate energy, increase shear, and reduce vortex strength similar to the BL MHV[39].

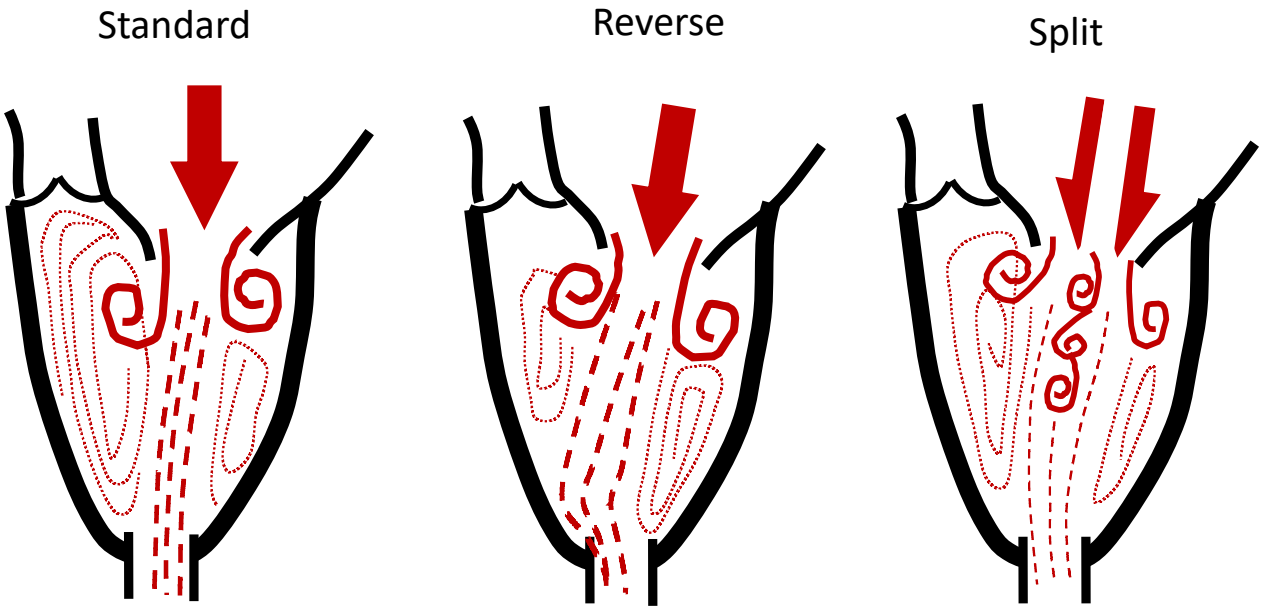

Figure 9. Illustrations of the intraventricular flow patterns observed in this study. The standard pattern exhibits a vortex ring in the midplane that grows asymmetrically towards the aortic valve. The reverse pattern results from inflow aimed at the septum, which allows the CCW vortex to grow. The split inflow dissipates energy but develops into an asymmetric vortex pattern. The majority of flow exited through the apical LVAD.

Previous publications reported that preexisting prosthesis MV (biological or mechanical) could be left in place upon LVAD implantation without any significant impacts on the pump function or TE risk, while special attention was needed to ensure proper anticoagulation management[14,19,21,40]. However, these practices are not well informed regarding the flow abnormalities, a gap which has been filled by the results of the present study. Higher LVAD support limited aortic valve opening, introducing larger regions of residual flow, especially around the aortic valve and left ventricular outflow tract. Further consideration of restoring intraventricular flow vortex behavior may result in new strategies for mitral repair and replacement for patients receiving LVADs.

Limitations

The cardiac simulator is a reproducible testbed for exploring the flow interaction of LVAD support with the native circulation, but has limitations on some aspects of physiological control, including lack of autoregulation and the Frank-Starling response. The system is open-loop, and the pressure equilibrated at the left atrial chamber and maintained constant throughout the study, thus preload alterations are not included in the system response and suction conditions are avoided. The dilated left

ventricle geometry is idealized from clinical measurements and is not a patient-specific model, but captures the significant features that govern the intraventricular flow dynamics[32,41]. While the blood analogue solution is standard for these studies, it does not replicate many features of blood including temperature-dependent rheology and coagulation. In addition, the relationship of vortex formation and fluid velocity in the left ventricular midplane does not capture the full three-dimensional nature of the flow field, or account for the T_R of particles as they pass through the chamber. The ensemble averaging imaging method utilized only 10 frames at each time point. The uncertainty of the average velocity fields at each time point was below 5%, except for the 5 frames during the early E-wave. In those frames, the maximum uncertainty was 25% and only visible in the mitral inflow region.

Conclusion

Intraventricular flow field indices for six different MV prosthesis designs/orientations under matched low cardiac output conditions during low and high LVAD support were measured in a cardiac simulator. The presence of the LVAD did not substantially alter the overall vortex formation. The BP valve provided the most natural intraventricular flow dynamics over the range of LVAD speeds while the TD-S severely impaired LV washout. This finding suggested that BL has a lower risk of thromboembolism for MHV in the mitral position, particularly in DCM patients that receive a LVAD. However, depending on the level of LVAD support level, optimizing the orientation of the BL valve may produce better flow mixing and transport.

Corresponding Author:
Dr. Karen May-Newman
Bioengineering Program
Department of Mechanical Engineering
San Diego State University
5500 Campanile Drive
San Diego, CA. 92182-1323, USA.
Email: kmaynewm@sdsu.edu

Conflicts of Interest Statement
The authors have no conflicts of interest to declare.

Funding Statement:
None

Data availability statement:
None

Acknowledgements
The authors appreciate the assistance of Juyeun Moon in conducting the experimental studies. The vortex analysis software was developed with Dr. Pablo Legazpi-Martinez and colleagues from the Hospital General Universitario Gregorio Marañón and Instituto de Investigación Sanitaria Gregorio Marañón, Madrid, Spain. The residence time software was developed with Dr. Juan Carlos del Alamo and Dr. Lorenzo Rossini from the Department of Mechanical and Aerospace Engineering at the University of California, San Diego. Many thanks to Abbott, Inc for the use of a HeartMate II LVAD and control system. Internal funding was used to support these studies.

References:

1. Nkomo VT, Gardin JM, Skelton TN, Gottdiener JS, Scott CG, Enriquez-Sarano M. Burden of valvular heart diseases: a population-based study. *Lancet (London, England)*. 2006;368(9540):1005-1011. doi: 10.1016/S0140-6736(06)69208-8

2. Hsich EM, Rogers JG, McNamara DM, et al. Does Survival on the Heart Transplant Waiting List Depend on the Underlying Heart Disease? *JACC Heart Fail*. 2016; 4(9):689-697. doi: 10.1016/j.jchf.2016.03.010

3. Park SJ, Tector A, Piccioni W, et al. Left ventricular assist devices as destination therapy: a new look at survival. *J Thorac Cardiovasc Surg*. 2005;129(1):9-17. doi: 10.1016/j.jtcvs.2004.04.044

4. Miller LW, Pagani FD, Russell SD, et al. Use of a continuous-flow device in patients awaiting heart transplantation. *N Engl J Med*. 2007;357(9):885-896. doi: 10.1056/NEJMoa067758

5. Robertson JO, Naftel DC, Myers SL, et al. Concomitant mitral valve procedures in patients undergoing implantation of continuous-flow left ventricular assist devices: An INTERMACS database analysis. *J Hear lung Transplant Off Publ Int Soc Hear Transplant*. 2018;37(1):79-88. doi: 10.1016/j.healun.2017.09.016

6. Vu V, Rossini L, Montes R, et al. Mitral Valve Prosthesis Design Affects Hemodynamic Stasis and Shear In The Dilated Left Ventricle. *Ann Biomed Eng*. 2019;47(5). doi: 10.1007/s10439-019-02218-z

7. Faludi R, Szulik M, D'hooge J, et al. Left ventricular flow patterns in healthy subjects and patients with prosthetic mitral valves: an in vivo study using echocardiographic particle image velocimetry. *J Thorac Cardiovasc Surg*. 2010;139(6):1501-1510. doi: 10.1016/j.jtcvs.2009.07.060

8. Pedrizzetti G, Domenichini F, Tonti G. On the left ventricular vortex reversal after mitral valve replacement. *Ann Biomed Eng*. 2010;38(3):769-773. doi: 10.1007/s10439-010-9928-2

9. Yin W, Alemu Y, Affeld K, Jesty J, Bluestein D. Flow-induced platelet activation in bileaflet and monoleaflet mechanical heart valves. *Ann Biomed Eng*. 2004;32(8):1058-1066. doi: 10.1114/B:ABME.0000036642.21895.3f

10. Yin W, Gallocher S, Pinchuk L, Schoephoerster RT, Jesty J, Bluestein D. Flow-induced platelet activation in a St. Jude mechanical heart valve, a trileaflet polymeric heart valve, and a St. Jude tissue valve. *Artif Organs*. 2005;29(10):826 -831. doi: 10.1111/j.1525-1594.2005.29109.x

11. Alemu Y, Bluestein D. Flow-induced Platelet Activation and Damage Accumulation in a Mechanical Heart Valve : Numerical Studies. 2007;31(9):677-688. doi: 10.1111/j.1525-1594.2007.00446.x

12. Bluestein D, Yin W, Affeld K, Jesty J. Flow-induced platelet activation in mechanical heart valves. *J Heart Valve Dis*. 2004; 13(3):501-508. http://www.ncbi.nlm.nih.gov/pubmed/15446502

13. Campos N. Comparison of the occurrence of thromboembolic and bleeding complications in patients with mechanical heart valve prosthesis with one and two leaflets in the mitral position. *Rev Bras Cir Cardiovasc*. 2014;29(1):59-68.

14. Schweiger M, Stepanenko A, Vierecke J, et al. Preexisting mitral valve prosthesis in patients undergoing left ventricular assist device implantation. *Artif Organs*. 2012; 36(1):49-53. doi: 10.1111/j.1525-1594.2011.01304.x

15. Lowe GD. Virchow's triad revisited: abnormal flow. *Pathophysiol Haemost Thromb*. 2003;33(5-6):455-457. doi: 83845

16. Barbone A, Rao V, Oz MC, Naka Y. LVAD support in patients with bioprosthetic valves. *Ann Thorac Surg*. 2002;74(1):232-234. doi: 10.1016/s0003-4975(01)03514-7

17. Schubmehl HB, Saric M, Vainrib AF, Williams M, Balsam LB. Rapid Bioprosthetic Mitral Valve Failure after Temporary Left Ventricular Assist Device Support. *Heart Surg Forum*. 2017; 20(6):E256-E257. doi: 10.1532/hsf.1861

18. Liu T, Jessup M, Acker M, Morris R. Management of prosthetic valves during ventricular assist device implantation. *J Card Surg*. 2010;25(5):601-605. doi: 10.1111/j.1540-8191.2010.01098.x

19. Krishan K, Pinney S, Anyanwu AC. Successful use of continuous flow ventricular assist device in a patient with mechanical mitral and aortic valve prosthesis without replacement or exclusion of valves. *Interact Cardiovasc Thorac Surg*. 2010;10(2):325-327. doi: 10.1510/icvts.2009.221036

20. Mussa S, Large S, Tsui S, van Doorn C, Jenkins D. Mechanical mitral prosthesis with a short-term left ventricular assist device. *ASAIO J*. 2008;54(4):439-441. doi: 10.1097/MAT.0b013e31817c921b

21. Mokashi SA, Schmitto JD, Lee LS, et al. Ventricular assist device in patients with prosthetic heart valves. *Artif Organs*. 2010;34(11):1030-1034. doi: 10.1111/j.1525-1594.2010.01102.x

22. Wong K, Samaroo G, Ling I, et al. Intraventricular flow patterns and stasis in the LVAD-assisted heart. *J Biomech*. 2014;47(6). doi: 10.1016/j.jbiomech.2013.12.031

23. Reider C, Moon J, Ramesh V, et al. Intraventricular thrombus formation in the LVAD-assisted heart studied in a mock circulatory loop. *Meccanica*. 2017;52(3). doi: 10.1007/s11012-016-0433-z

24. Williams MR, Oz MC. Indications and patient selection for mechanical ventricular assistance. *Ann Thorac Surg*. 2001;71(3 Suppl):S86-91; discussion S114 -5. doi: 10.1016/s0003-4975(00)02627-8

25. Ky B, French B, May Khan A, et al. Ventricular-arterial coupling, remodeling, and prognosis in chronic heart failure. *J Am Coll Cardiol*. 2013;62(13):1165-1172. doi: 10.1016/j.jacc.2013.03.085

26. Bermejo J, Benito Y, Alhama M, et al. Intraventricular vortex properties in non-ischemic dilated cardiomyopathy. *Am J Physiol Hear Circ Physiol*. 2014;306(5): H718-29. doi: 10.1152/ajpheart.00697.2013

27. Rossini L, Martinez-Legazpi P, Vu V, et al. A clinical method for mapping and quantifying blood stasis in the left ventricle. *J Biomech*. 2016;49(11):2152-2161. doi: 10.1016/j.jbiomech.2015.11.049

28. Querzoli G, Fortini S, Cenedese A. Effect of the prosthetic mitral valve on vortex dynamics and turbulence of the left ventricular flow. *Phys Fluids*. 2010;22(4):1-10. doi: 10.1063/1.3371720

29. Kilner PJ, Yang GZ, Wilkes a J, Mohiaddin RH, Firmin DN, Yacoub MH. Asymmetric redirection of flow through the heart. *Nature*. 2000;404(6779):759-761. doi: 10.1038/35008075

30. Martinez-Legazpi P, Bermejo J, Benito Y, et al. Contribution of the diastolic vortex ring to left ventricular filling. *J Am Coll Cardiol*. 2014;64(16):1711-1721. doi: 10.1016/j.jacc.2014.06.1205

31. Pierrakos O, Tech V, Alley M, Telionis D. Vortex Dynamics and Energetics in Left Ventricular Flows Vortex Dynamics and Energetics in Left Ventricular Flows. *Heart*. Published online 2006.

32. Pedrizzetti G, Domenichini F. Nature Optimizes the Swirling Flow in the Human Left Ventricle. *Phys Rev Lett*. 2005;95(10):1-4. doi: 10.1103/PhysRevLett.95.108101

33. Hendabadi S, Bermejo J, Benito Y, et al. Topology of blood transport in the human left ventricle by novel processing of Doppler echocardiography. *Ann Biomed Eng*. 2013;41(12):2603-2616. doi: 10.1007/s10439-013-0853-z

34. Alexandru G. Fredriksson, Jakub Zajac JE. 4-D blood flow in the human right ventricle. *Am J Physiol Hear Circ Physiol*. 2011;301:H2344-H2350. doi: 10.1152/ajpheart.00622.2011.

35. Bermejo J, Benito Y, Alhama M, et al. Intraventricular vortex properties in nonischemic dilated cardiomyopathy. *Am J Physiol Heart Circ Physiol*. 2014;306(5):H718-29. doi: 10.1152/ajpheart.00697.2013

36. Fredriksson AG, Svalbring E, Eriksson J, et al. 4D flow MRI can detect subtle right ventricular dysfunction in primary left ventricular disease. *J Magn Reson Imaging*. 2016;43(3):558-565. doi: 10.1002/jmri.25015

37. Rossini L, Martinez-Legazpi P, Benito Y, et al. Clinical assessment of intraventricular blood transport in patients undergoing cardiac resynchronization therapy. *Meccanica*. 2017;52(3). doi: 10.1007/s11012-015-0322-x

38. Okafor I, Santhanakrishnan A, Raghav V, Yoganathan AP. Role of Mitral Annulus Diastolic Geometry on Intraventricular Filling Dynamics. *J Biomech Eng*. 2015;137(December):1-9. doi: 10.1115/1.4031838

39. Bloodworth CH 4th, Pierce EL, Kohli K, et al. Impact of simulated MitraClip on forward flow obstruction in the setting of mitral leaflet tethering: An in vitro investigation. *Catheter Cardiovasc Interv Off J Soc Card Angiogr Interv*. 2018;92(4):797-807. doi: 10.1002/ccd.27692

40. Rao V, Slater JP, Edwards NM, Naka Y, Oz MC. Surgical management of valvular disease in patients requiring left ventricular assist device support. *Ann Thorac Surg*. 2001;71(5):1448-1453. doi: S0003-4975(01)02479-1 [pii]

41. Domenichini F, Querzoli G, Cenedese A, Pedrizzetti G. Combined experimental and numerical analysis of the flow structure into the left ventricle. *J Biomech*. 2007;40(9):1988-1994. doi: 10.1016/j.jbiomech.2006.09.024